Journal of Molecular Structure 1336 (2025) 142137

Contents lists available at ScienceDirect

Journal of Molecular Structure

journal homepage: www.elsevier.com/locate/molstr

Advancing the coordination abilities of 2,6-diacetylpyridine bis (benzoylhydrazone) with tin through modifications of axial ligands: Synthesis, spectroscopic features, and structural profiling

Tushar S. Basu Baul [a,*], Avishek Khatiwara [a], Amon Das [a], Andrew Duthie [b], Sean Parkin [c,*]

[a] Centre for Advanced Studies in Chemistry, North-Eastern Hill University, NEHU Permanent Campus, Umshing, Shillong 793 022, India
[b] School of Life & Environmental Science, Deakin University, Pigdons Road, Waurn Ponds, Victoria 3216, Australia
[c] Department of Chemistry, University of Kentucky, 506 Library Drive, 146 Chemistry-Physics Building, Lexington, KY 40506-0055, USA

ARTICLE INFO

Keywords:
Schiff-base
Pentadentate ligands
Pentagonal-bipyramidal
Sn(IV) complexes,
Spectroscopy
Crystal structure

ABSTRACT

A series of seven-coordinate pentagonal-bipyramidal (PBPY-7) Sn(IV) complexes with the pentadentate pyridine-based pro-ligand 2,6-diacetylpyridine bis(benzoylhydrazone), H_2L, and different axial ligands have been synthesized. Reactions of H_2L with R_2SnO (where R = Me, *n*-Bu, *n*-Oct, or Bz) in anhydrous toluene, or with $RSnCl_3$ (where R = *n*-Bu or Ph) in anhydrous toluene (or acetonitrile in the case of $PhSnCl_3$), produced a series of novel seven-coordinate complexes: [$Me_2Sn(L)$] (**1**), [*n*-$Bu_2Sn(L)$] (**2**), [*n*-$Oct_2Sn(L)$] (**3**), [$Bz_2Sn(L)$] (**4**), [*n*-BuSn(L)Cl]·$0.5C_7H_8$ (**5**), and [PhSn(L)Cl] (**6**). By taking advantage of lability of the axial Cl ligands in complex **5**, two neutral PBP Sn(IV) complexes [*n*-BuSn(L)N_3] (**7**) and [*n*-BuSn(L)NCS] (**8**) with different axial ligands were obtained and characterized. In a separate effort to obtain single crystals of the dibenzyltin compound [$Bz_2Sn(L)$] (**4**), a few crystals were successfully extracted from crystallization experiments in chloroform. Diffraction studies of these crystals revealed a composition of [$Sn(L)Cl_2$]·$CHCl_3$ (**9**). In these complexes, the double-deprotonated chelating ligand occupies the equatorial plane, while the two axial ligands can be two R groups, two Cl ligands, or a combination of one R group with a Cl, N_3, or NCS ligand. The compounds **1**–**8** (**9** only by IR) were fully characterized using Fourier transform infrared (FT-IR) spectroscopy, high-resolution mass spectrometry (HRMS), and solution-state Fourier transform nuclear magnetic resonance (FT-NMR) spectroscopy. Single crystal X-ray diffraction analysis confirmed that all complexes **1**–**9** exhibit a PBP geometry. Notably, all complexes display significant in-plane distortion of the SnN_3O_2 pentagon due to shifts in the Sn(IV) ion position.

1. Introduction

Schiff bases are considered privileged ligands due to their highly modular synthesis, which allows for precise control over donor atoms, denticity, chelating ability, as well as electronic and steric properties. Consequently, their metal complexes have been extensively studied for their unique physico-chemical and structural properties, including notable catalytic activity, selectivity, and stability [1,2]. Schiff-base ligands and their metal complexes with N_3O_2 and N_2O_3 donor sets are among the most frequently investigated due to their intriguing spin crossover phenomena [3–6].

Among these, the 2,6-diacetylpyridine bis(acylhydrazone) ligands stand out because they feature at least five donor atoms (N_3O_2) arranged in a way that facilitates the formation of seven-coordinated complexes with a pentagonal-bipyramidal (PBPY-7) geometry. While this PBPY-7 geometry is commonly observed with these ligands, other geometries have also been documented [7]. The specific geometry of the complex depends on various factors, including the central metal ion, the conformational flexibility of the hydrazone ligand, and the reaction conditions [8]. Furthermore, the acidity of the hydrazone group in these ligands adds to the structural versatility of the resulting metal complexes, allowing for coordination in non-deprotonated, partially deprotonated, or fully deprotonated forms [9].

The growing interest in transition metal and lanthanide complexes of 2,6-diacetylpyridine bis(acylhydrazone) ligands is driven by their potential in advanced molecular magnetic applications. These complexes

* Corresponding authors.
E-mail addresses: basubaul@nehu.ac.in (T.S. Basu Baul), s.parkin@uky.edu (S. Parkin).

https://doi.org/10.1016/j.molstruc.2025.142137
Received 22 January 2025; Received in revised form 16 March 2025; Accepted 21 March 2025
Available online 22 March 2025

show significant promise as single-molecule magnets (SMMs) and single-chain magnets (SCMs) [10–12]. Beyond their magnetic properties, metal complexes of these ligands with a PBPY-7 have also demonstrated a wide range of biological activities. These activities include cytotoxicity against various cell lineages [13–15], superoxide dismutase (SOD) mimetic activity [16–18], and interactions with DNA/RNA, which can include nuclease activity [19–21] and antimicrobial properties [22–25].

The chemistry of tin complexes with 2,6-diacetylpyridine bis(acylhydrazone) ligands is relatively unexplored compared to the chemistry of transition metals, main group metals, actinides, and lanthanides, with only a few examples characterized crystallographically, such as [*n*-Pr_2Sn(L)] (L = 2,6-diacetylpyridine bis(2-hydroxybenzoylhydrazone)) [26], [*n*-BuSnCl(L^1)], and [Ph_2Sn(L^1)] (L^1 = 2,6-diacetylpyridine bis(2-aminobenzoylhydrazone)) [27], [Sn(L^2)Cl_2]·H_2O (L^2 = 2,6-diacetylpyridine bis(picolinoylhydrazone)) [28], the ionic complex [Et_2Sn(H_2L^3)][Et_2SnCl_3]Cl_3·H_2O (L^3 = 2,6-diacetylpyridine bis(isonicotinoylhydrazone)) [23] and the neutral tin(II) complex [Sn(L)(H_2O)$_2$]·4H_2O, with the latter being obtained through an electrochemical procedure [29]. Although the literature contains only one report on tin(IV) complexes of 2,6-diacetylpyridine bis(benzoylhydrazone), the details on synthesis, isolation, and crystallographic characterization are lacking. In some instances, tin NMR was employed to predict the structures [30]. Recently, we reported neutral tin(IV) complexes using R_2SnO (R = Me, *n*-Bu, *n*-Oct, Bz) and $RSnCl_3$ (R = *n*-Bu or Ph) with the quinquedentate pro-ligand 2,6-diacetylpyridine bis(2-hydroxybenzoylhydrazone), finding this method effective for preparing seven-coordinated tin complexes. Consequently, we recently reported two types of neutral complexes: [R_2Sn(L)] and [RSn(L)Cl] [31]. These complexes frequently adopt a PBPY-7 geometry around the central tin atom. Thus, the flexibility in axial ligand substitution in PBPY-7 tin complexes adds an extra layer of tunability, enabling the creation of complex, highly functionalized structures for diverse applications, such as catalysis and materials science, and biological applications. To advance our research, we have redirected our attention to 2,6-diacetylpyridine bis(benzoylhydrazone), H_2L, for the synthesis of various organotin derivatives: [Me_2Sn(L)] (**1**), [*n*-Bu_2Sn(L)] (**2**), [*n*-Oct_2Sn(L)] (**3**), [Bz_2Sn(L)] (**4**), [*n*-BuSn(L)Cl]·0.5C_7H_8 (**5**), [PhSn(L)Cl] (**6**), [*n*-BuSn(L)N_3] (**7**), [*n*-BuSn(L)NCS] (**8**) and [Sn(L)Cl_2]·$CHCl_3$ (**9**).

2. Experimental

Materials, physical measurements, and the synthesis of the pro-ligand 2,6-diacetylpyridine bis(benzoylhydrazone) (**H_2L**) are presented in ESI Text S1.

2.1. Synthesis of organotin(IV) compounds *1*–*9*

The preparation of organotin(IV) compounds **1**–**9** (as depicted in Scheme 1), was carried out following the four general synthetic pathways outlined below.

2.1.1. Synthesis of [Me_2Sn(L)] *1*

Me_2SnO (0.12 g, 0.75 mmol) was added to a suspension containing H_2L (0.3 g, 0.75 mmol) in 50 mL of anhydrous toluene in a round-bottom flask fitted with a Dean-Stark moisture trap. The reaction mixture was heated to reflux for approximately 4 h. As the reaction progressed, the mixture gradually developed a pale yellow color and became clear. The solution was filtered while still hot, and the volatiles were removed using a rotary evaporator. The residue was washed with hexane (3 × 1 mL) and dried *in vacuo*. Several recrystallizations using benzene, followed by the slow evaporation of a clear solution, resulted in the formation of a pale yellow crystalline product. Yield: 48 % (0.2 g). M. p.: > 300 °C. FT-IR (ATR mode; ν in cm^{-1}): 1584 (w) $\nu(CN)_{imine}$, 1548 (w) $\nu(C{=}N)_{py}$, 1503 (vs), 1429 (m), 1358 (vs), 1324 (s), 1296 (s), 1168 (s),

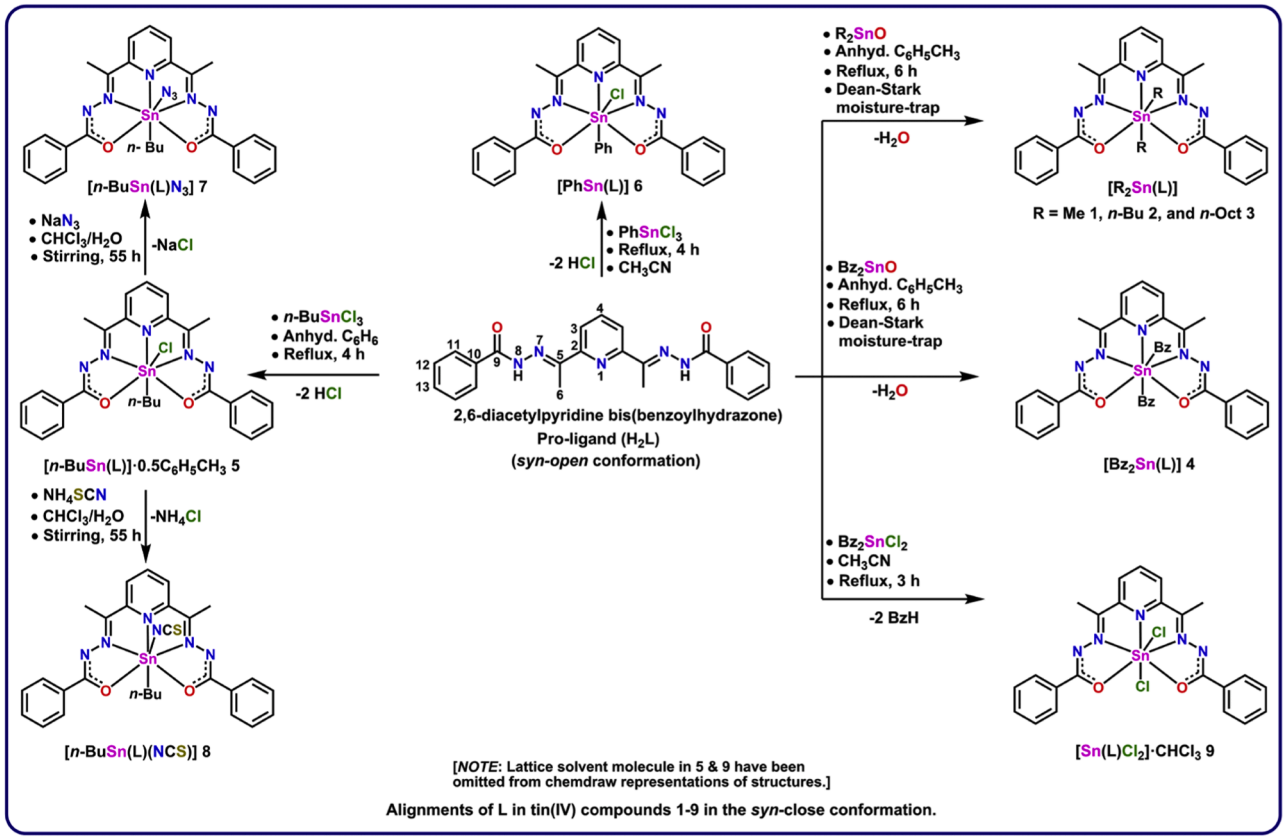

Scheme 1. Reaction sequences for synthesizing tin compounds, including the alignment of ligand L^{2-} in compounds **1**–**9** as observed in the solid state along with the atom numbering of the pro-ligand used for the assignment of the NMR signals.

1052 (m), 996 (m) ν(N—N), 903 (m), 808 (s), 714 (vs), 678 (vs), 651 (m), 572 (m). ^{1}H NMR (400.13 MHz, $CDCl_3$): δ = 8.43 (d, 4H, H-11), 8.16 (t, 1H, H-4), 7.81(d, 2H, H-3), 7.46 (m, 6H, H-12, H-13), 2.75 (s, 6H, H-6), 0.31 (s, $^{2}J(^{1}H\text{-}^{119}Sn)$ 116 Hz, 6H, MeSn) ppm. ^{13}C NMR (100.62 MHz, $CDCl_3$): δ = 173.01 (C-9, C—O), 149.14 (C-2, C═N), 144.98 (C-5, C═N), 141.27, 135.59, 130.99, 128.97, 127.93, 121.58, 12.86 (C-6), 12.03 (MeSn). ^{119}Sn NMR (149.15 MHz, $CDCl_3$): δ = − 433.8 ppm. HRMS-ESI^{+} (*m/z*, %): found 548.1101 (100); calcd. for $[M + H]^{+}$548.1108.

2.1.2. Synthesis of [n-Bu$_2$Sn(L)] **2**

A method similar to that used for preparing compound **1** was applied, utilizing *n*-Bu_2SnO (0.186 g, 0.75 mmol) and H_2L (0.3 g, 0.75 mmol). After filtration, the resulting solution was concentrated to one-third of its original solvent volume, which upon slow evaporation at room temperature, yielded orange crystalline material of compound **2**. Yield: 70 % (0.33 g); M. p.: 236–237 °C. FT-IR (ATR mode; ν in cm^{-1}): 2908 (m) $\nu(C—H)_{aliphatic}$, 1588 (m) $\nu(CN)_{imine}$, 1547 (m) $\nu(C═N)_{py}$, 1499 (s), 1426 (m), 1356 (vs), 1319 (s), 1295 (s), 1166 (s), 1047 (s), 992 (m) ν(N—N), 900 (m), 803 (s), 710 (s), 680 (vs), 621 (w), 550 (w), 527 (w). ^{1}H NMR (400.13 MHz, $CDCl_3$): δ = 8.41 (d, 4H, H-11), 8.17 (t, 1H, H-4), 7.81 (d, 2H, H-3), 7.47 (m, 6H, H-12, H-13), 2.76 (s, 6H, H-6), 0.96 (m, 12H, *n*-BuSn-1/2/3), 0.56 (t, 6H, *n*-BuSn-4) ppm. ^{13}C NMR (100.62 MHz, $CDCl_3$): δ = 173.43 (C-9, C—O), 149.73 (C-2, C═N), 145.23 (C-5, C═N), 141.13, 135.84, 130.86, 128.96, 127.93, 121.39, 30.40 (*n*-BuSn-2), 27.32 (*n*-BuSn-3), 26.22 (*n*-BuSn-1), 13.51 (*n*-BuSn-4), 12.85 (C-6) ppm. ^{119}Sn NMR (149.15 MHz, $CDCl_3$): δ = − 440.2 ppm. HRMS-ESI^{+} (*m/z*, %): found 632.1987 (100); calcd. for $[M + H]^{+}$632.2047.

2.1.3. Synthesis of [n-Oct$_2$Sn(L)] **3**

A method similar to that used for preparing compound **1** was applied, utilizing *n*-Oct_2SnO (0.18 g, 0.50 mmol) and H_2L (0.2 g, 0.50 mmol). After filtration, the volatiles were removed using a rotary evaporator. The residue was washed with hexane (3 × 1 mL), dried *in vacuo*, and extracted by boiling with dichloromethane. The dichloromethane extract was concentrated to a minimum volume, and hexane was added to induce precipitation. The resulting solid was collected by filtration. This dissolution and precipitation procedure was repeated at least three times. Recrystallization from a toluene/ethanol mixture yielded orange crystalline material of compound **3**. Yield: 75 % (0.28 g); M. p.: 134–135 °C. FT-IR (ATR mode; ν in cm^{-1}): 2922 (w) $\nu(C—H)_{aliphatic}$, 1586 (w) $\nu(CN)_{imine}$, 1548 (w) $\nu(C═N)_{py}$, 1500 (s), 1357 (vs), 1324 (s), 1297 (m), 1170 (s), 1049 (s), 993 (w) ν(N—N), 902 (w), 815 (s), 745 (w), 713 (vs), 679 (vs), 652 (w), 550 (w), 524 (w). ^{1}H NMR (400.13 MHz, $CDCl_3$): δ = 8.26 (d, 4H, H-11), 8.01 (t, 1H, H-4), 7.65 (d, 2H, H-3), 7.32 (m, 6H, H-12, H-13), 2.61 (s, 6H, H-6), 0.95 (m, 4H, *n*-OctSn-1), and 0.85 (m, 24H, *n*-OctSn-2/3/4/5/6/7), 0.61 (t, 6H, *n*-OctSn-8) ppm. ^{13}C NMR (100.62 MHz, $CDCl_3$): δ = 173.40 (C-9, C—O), 149.70 (C-2, C═N), 145.23 (C-5, C═N), 141.12, 135.79, 130.84, 128.93, 127.91, 121.37, 33.15 (*n*-OctSn-3), 31.70 (*n*-OctSn-6), 30.53 (*n*-OctSn-5), 29.09 (*n*-OctSn-4), 28.89 (*n*-OctSn-1), 25.09 (*n*-OctSn-2), 22.53 (*n*-OctSn-7), 14.01 (*n*-OctSn-8), 12.85 (C-6) ppm. ^{119}Sn NMR (149.15 MHz, $CDCl_3$): δ = − 440.2 ppm. HRMS-ESI^{+} (*m/z*, %): found 744.3116 (75); calcd. for $[M + H]^{+}$744.3299.

2.1.4. Synthesis of [Bz$_2$Sn(L)] **4**

A method similar to that used for preparing compound **1** was applied, utilizing Bz_2SnO (0.11 g, 0.37 mmol) and H_2L (0.15 g, 0.37 mmol). After filtration, the resulting solution was concentrated to one-third of its original solvent volume, which upon slow evaporation at room temperature, yielded orange crystalline material of compound **4**. Yield: 38 % (0.1 g); M. p.: 225–226 °C. FT-IR (ATR mode; ν in cm^{-1}): 2933 (w) $\nu(C—H)_{aliphatic}$, 1585 (w) $\nu(CN)_{imine}$, 1555 (w) $\nu(C═N)_{py}$, 1498 (s), 1418 (w), 1360 (vs), 1329 (s), 1298 (s), 1173 (s), 1052 (s), 996 (w) ν(N—N), 901 (w), 798 (s), 764 (s), 708 (vs), 680 (vs), 554 (w), 529 (w). ^{1}H NMR (400.13 MHz, $CDCl_3$): δ = 8.48 (d, 4H, H-11), 7.78 (t, 1H, H-4), 7.52 (m, 6H, H-12, H-13), 7.27 (d, 2H, H-3), 6.61 (m, 6H, BzSn-4,5), 6.21 (d, 4H, BzSn-3), 2.48 (s, $^{2}J(^{1}H\text{-}^{119}Sn)$ 117 Hz, 4H, BzSn-1), 2.42 (s, 6H, H-6) ppm. ^{13}C NMR (100.62 MHz, $CDCl_3$): δ = 172.76 (C-9, C—O), 148.51 (C-2, C═N), 146.00 (C-5, C═N), 140.72, 140.54, 135.60 (BzSn-2), 131.08, 129.01, 128.01, 126.81 ($^{4}J(^{13}C\text{-}^{117/119}Sn)$ 27 Hz, BzSn-4), 126.70 ($^{3}J(^{13}C\text{-}^{119}Sn)$ 50 Hz, BzSn-3), 122.86 ($^{3}J(^{13}C\text{-}^{119}Sn)$ 43 Hz, BzSn-5), 120.77, 38.22 (BzSn-1), 12.61 (C-6) ppm. ^{119}Sn NMR (149.15 MHz, $CDCl_3$): δ = − 491.4 ppm. HRMS-ESI^{+} (*m/z*, %): found 700.2179 (100); calcd. for $[M + H]^{+}$700.1734.

2.1.5. Synthesis of [n-BuSn(L)Cl]·0.5C$_7$H$_8$ **5**

A toluene solution (20 mL) containing *n*-$BuSnCl_3$ (0.14 g, 0.50 mmol) was slowly added dropwise to a stirred suspension of H_2L (0.2 g, 0.50 mmol) in anhydrous toluene (20 mL), followed by reflux for 4 h. During this time, the heterogeneous mixture became clear. It was then filtered while still hot to remove any suspended particles. The resulting yellow solution was concentrated to one-third of its original solvent volume using a rotary evaporator. After standing at room temperature, yellow microcrystalline material formed. The crystals were separated from the mother liquor, thoroughly rinsed with hexane (4 × 1 mL), and dried *in vacuo*. Yield: 27 % (0.18 g). M. p.: >300 °C. FT-IR (ATR mode; ν in cm^{-1}): 2919 (w) $\nu(C—H)_{aliphatic}$, 1581 (w) $\nu(CN)_{imine}$, 1554 (w) $\nu(C═N)_{py}$, 1499 (s), 1417 (w), 1375 (vs), 1329 (m), 1298 (w), 1166 (s), 1052 (m), 1024 (w) ν(N—N), 1000 (w), 937 (w), 903 (w), 811 (s), 712 (vs), 686 (vs), 656 (m), 537 (m). ^{1}H NMR (400.13 MHz, $CDCl_3$): δ = 8.46 (d, 4H, H-11), 8.22 (t, 1H, H-4), 7.85 (d, 2H, H-3), 7.49 (m, 6H, H-12, H-13), 2.78 (s, 6H, H-6), 1.01 (m, 4H, *n*-BuSn-1,2), 0.87 (m, 2H, *n*-BuSn-3), 0.58 (t, 3H, *n*-BuSn-4) ppm. ^{13}C NMR (100.62 MHz, $CDCl_3$): δ = 172.59 (C-9, C—O), 146.70 (C-2, C═N), 144.31 (C-5, C═N), 142.43, 134.08, 131.73, 129.12, 128.00, 122.48, 29.53 (*n*-BuSn-2), 26.89 (*n*-BuSn-3), 25.90 (*n*-BuSn-1), 13.40 (*n*-BuSn-4), 13.11 (C-6) ppm. ^{119}Sn NMR (149.15 MHz, $CDCl_3$): δ = – 565.7 ppm. HRMS-ESI^{+} (*m/z*, %): found 610.1041 (79); calcd. for $[M + H]^{+}$610.1032.

2.1.6. Synthesis of [PhSn(L)Cl] **6**

A solution of acetonitrile (20 mL) containing $PhSnCl_3$ (0.15 g, 0.50 mmol) was added dropwise to a stirred solution of H_2L (0.2 g, 0.50 mmol) in acetonitrile (40 mL) at room temperature. The reaction mixture was then stirred in an oil bath at 80 °C for 3 h, during which it turned yellow. The yellow solution was filtered and concentrated to one-third of its original volume using a rotary evaporator. After standing at room temperature, a pale yellow microcrystalline material was obtained. The product was rinsed with hexane (4 × 1 mL) and dried *in vacuo*. Yield: 45 % (0.14 g); M. p.: > 300 °C. FT-IR (ATR mode; ν in cm^{-1}): 1580 (w) $\nu(CN)_{imine}$, 1553 (w) $\nu(C═N)_{py}$, 1501 (s), 1418 (w), 1376 (vs), 1327 (m), 1300 (m), 1268 (w), 1168 (s), 1054 (m), 999 (m) ν(N—N), 904 (m), 809 (s), 711 (vs), 688 (vs), 658 (m), 556 (m), 540 (m). ^{1}H NMR (400.13 MHz, $CDCl_3$): δ = 8.48 (d, 4H, H-11), 8.16 (t, 1H, H-4), 7.83 (d, 2H, H-3), 7.51 (m, 6H, H-12, H-13), 7.02 (m, 5H, PhSn-2,3,4), 2.83 (s, 6H, H-6) ppm. ^{13}C NMR (100.62 MHz, $CDCl_3$ + DMSO-d_6): δ = 169.56 (C-9, C—O), 147.16 (C-2, C═N), 145.03 (C-5, C═N), 143.49, 142.18, 131.76, 130.21, 130.16, 126.83, 126.73, 126.63, 126.47, 122.93, 11.54 (C-6) ppm. ^{119}Sn NMR (149.15 MHz, $CDCl_3$): δ = – 612.2 ppm. HRMS-ESI^{+} (*m/z*, %): found 630.0568 (100); calcd. for $[M + H]^{+}$630.0719.

2.1.7. Synthesis of [n-BuSn(L)N$_3$] **7**

Starting compound [*n*-BuSn(L)Cl] **5** (0.2 g, 0.49 mmol) was dissolved in chloroform (50 mL). Sodium azide (0.1 g, 0.49 mmol) in water (5 mL) was then added while stirring, and the resulting biphasic reaction mixture was stirred for 55 h. The aqueous phase was separated and washed with water (2 × 15 mL). The combined yellow organic phases were dried over anhydrous sodium sulfate. After filtration, the clear solution of the product was concentrated to a minimal volume, yielding a yellow microcrystalline solid. This solid was then recrystallized from anhydrous benzene to obtain the desired product. Yield: 40 % (0.08 g).

Note: Although no incident occurred while using azide during preparation and isolation, care in handling azides must be exercised owing to their potentially explosive nature. FT-IR (ATR mode; ν in cm^{-1}): 2917 (w) $\nu(C—H)_{aliphatic}$, 2065 (vs) $\nu(N_3)$, 1584 (w) $\nu(CN)_{imine}$, 1553 (w) $\nu(C═N)_{py}$, 1449 (vs), 1415 (w), 1370 (vs), 1330 (w), 1293 (w), 1180 (s), 1054 (s), 999 (m) ν(N—N), 904 (m), 806 (m), 715 (vs), 686 (s), 657 (w), 535 (m). ^{1}H NMR (400.13 MHz, $CDCl_3$): δ = 8.36 (d, 4H, H-11), 8.17 (t, 1H, H-4), 7.81 (d, 2H, H-3), 7.43 (m, 6H, H-12, H-13), 2.73 (s, 6H, H-6), 0.96 (m, 4H, *n*-BuSn-1,2), 0.86 (m, 2H, *n*-BuSn-3), 0.52 (t, 3H, *n*-BuSn-4) ppm. ^{13}C NMR (100.62 MHz, $CDCl_3$): δ = 172.55 (C-9, C—O), 146.64 (C-2, C═N), 144.35 (C-5, C═N), 142.46, 134.06, 131.71, 129.09, 127.99, 122.50, 29.52 (*n*-BuSn-2), 26.88 (*n*-BuSn-3), 25.89 (*n*-BuSn-1), 13.40 (*n*-BuSn-4), 13.10 (C-6) ppm. ^{119}Sn NMR (149.08 MHz, $CDCl_3$): δ = – 558.6 ppm. HRMS-ESI$^+$ (*m/z*, %): found 574.2094 (100); calcd. for $[M - N_3]^+$ 574.1265; found 617.2439 (2.6); calcd. for $[M + H]^+$ 617.1435.

2.1.8. Synthesis of [n-BuSn(L)(NCS)] 8

A method similar to that used for preparing compound **7** was employed, utilizing [*n*-BuSn(L)Cl] (**5**) (0.16 g, 0.26 mmol) and ammonium thiocyanate (0.1 g, 1.31 mmol). After the work-up procedure and recrystallization from benzene, the product was isolated as pale yellow crystals. Yield: 0.14 g (70 %), M. p.: 275–276 °C. FT-IR (ATR mode; ν in cm^{-1}): 2920 (w) $\nu(C—H)_{aliphatic}$, 2065 (vs) ν(NCS), 1584 (w) $\nu(CN)_{imine}$, 1553 (w) $\nu(C═N)_{py}$, 1501 (vs), 1416 (w), 1372 (vs), 1330 (s), 1302 (m), 1182 (s), 1055 (m), 1000 (w) ν(N—N), 906 (m) ν(C-S), 804 (m), 715 (vs), 687 (s), 536 (w). ^{1}H NMR (400.13 MHz, $CDCl_3$): δ = 8.37 (d, 4H, H-11), 8.20 (t, 1H, H-4), 7.85 (d, 2H, H-3), 7.45 (m, 6H, H-12, H-13), 2.75 (s, 6H, H-6), 0.94 (m, 4H, *n*-BuSn-1,2), 0.81 (m, 2H, *n*-BuSn-3), 0.51 (t, 3H, *n*-BuSn-4) ppm. ^{13}C NMR (100.62 MHz, $CDCl_3$): δ = 173.05 (C-9, C—O), 146.82 (C-2, C═N), 145.47 (C-5, C═N), 142.81, 133.62, 131.99, 129.09, 128.12, 122.65, 30.92 (acetone), 28.41 (*n*-BuSn-2), 26.64 (*n*-BuSn-3), 25.75 (*n*-BuSn-1), 13.33 (*n*-BuSn-4), 13.01 (C-6) ppm. ^{119}Sn NMR (149.08 MHz, $CDCl_3$): δ = – 599.1 ppm. HRMS-ESI$^+$ (*m/z*, %): found 574.1479 (100); calcd. for $[M - NCS]^+$; 574.1265; found 633.1344 (3.8); calcd. for $[M + H]^+$ 633.1095.

2.1.9. Synthesis of [Sn(L)Cl2]·CHCl3 9

Compound **9** was obtained from an attempted reaction where 10 mL of an acetonitrile solution containing Bz_2SnCl_2 (0.18 g, 0.50 mmol) was added to a hot, stirred solution of H_2L (0.2 g, 0.50 mmol) in 30 mL of acetonitrile, aiming to produce [Bz_2Sn(L)] **4**. After evaporating the solvent, a crude material was obtained. Attempts to dissolve the crude material in chloroform through successive heating and filtration provided a few yellow crystals. M. p.: > 300 °C. FT-IR (ATR mode; ν in cm^{-1}): 1583 (w) $\nu(CN)_{imine}$, 1554 (w) $\nu(C═N)_{py}$, 1497 (s), 1361 (vs), 1328 (m), 1298 (m), 1172 (m), 1052 (m), 1024 (w) ν(N—N), 995 (w), 901 (m), 798 (m), 764 (s), 708 (s), 680 (s), 554 (m). Diffraction studies were conducted on the isolated yellow crystals, indicating a composition of [Sn(L)Cl_2]·$CHCl_3$ (see X-ray discussion). Several reaction trials to obtain more of **9** were unsuccessful and the product could not be reproduced.

2.2. X-ray crystallography

Single crystals of compounds **1**–**9** were grown by slow evaporation of various solvent systems, namely: **1** (dichloromethane/hexane, 2:1, v/v); **2** (toluene); **3** (benzene/ethanol, 2:1, v/v); **4** (toluene/chloroform, 1:2, v/v); **5** (toluene/ethanol (2:1, v/v); **6** (acetonitrile); **7** (acetone); **8** (benzene); **9** (chloroform). For each sample, a suitable crystal was mounted from oil (polyisobutene) on a fine glass fiber and flash-cooled [32] to either 100 K or 180 K (**2** only, to avoid a destructive phase transition). Diffraction data were collected using a dual microsource Bruker D8 Venture diffractometer using *MoKα* ($\lambda = 0.71073$Å) or *CuKα* ($\lambda = 1.54178$Å) radiation (latter for **4** only). Data collection and reduction [33], absorption correction [34,35], structure solution [36], refinement [37], and validation [38,39] were by published methods. Crystals of **1** and **6** were twinned by reticular pseudo-merohedry and inversion, respectively, see e.g. in ref [40]. Data for **1** were processed following the recommendations of Sevvana et al. [41]. Crystals of **2, 5**, and **8** had disorder of side-chains attached to their Sn atom, which was refined using separate PARTs in *SHELXL* [37]. Lastly, crystals of **7** and **8** had severely disordered solvent occupying channels that was factored out of the refinement by the *SQUEEZE* routine in *Platon* [42].

3. Results and discussion

3.1. Synthesis and spectroscopy

We commenced our research into systematically developing synthetic methods for producing various organotin compounds featuring a pentagonal bipyramidal geometry, facilitated by N_3O_2 donor atoms arranged in a pentagonal coordination plane. To begin, we used the well-known pro-ligand, 2,6-diacetylpyridine bis(benzoylhydrazone) (H_2L), which we prepared by condensing 2,6-diacetylpyridine with two equivalents of benzoylhydrazine in ethanol, with minor modifications. The purity and integrity of the product was assessed using HRMS results. H_2L is soluble in polar solvents such as acetonitrile, DMF, and DMSO. The ^{1}H NMR spectrum of H_2L in DMSO-d_6 solution exhibited a consistent integral ratio among the NH, methyl singlet, and broad aromatic signals. The characteristic IR vibrations are included in the Experimental section, along with other data. Diorganotin(IV) complexes of formulations [R_2Sn(L)] **1**–**4** were synthesized by refluxing equimolar amounts of the corresponding R_2SnO and H_2L in toluene, following the removal of water. The gradual color change to yellow signaled the formation of complexes. The reactions of monoorganotin(IV) trihalides, such as *n*-$BuSnCl_3$ and $PhSnCl_3$, with H_2L in benzene or acetonitrile resulted in the formation of [*n*-BuSn(L)Cl] **5** and [PhSn(L)Cl] **6**. Compounds **5** and **6** contain a neutral deprotonated equatorial ligand, *n*-Bu (or Ph) and Cl^- ligands in axial positions. Organotin azide [*n*-BuSn(L)N_3] **7** was prepared by reaction of [*n*-BuSn(L)Cl] **5** with an excess of sodium azide in a water/chloroform biphasic mixture (Scheme 1). An analogous method to that of azido compound **7** was employed, involving NH_4SCN and compound **5**, which upon suitable workup, generated isothiocyanato compound [*n*-BuSn(L)NCS] **8**. To our knowledge, complexes **7** and **8** represent the first examples of PBPY-7 tin(IV) complexes of L with azido/isothiocyanato ligand(s) and monoorganotin(IV) compounds with axial locations.

The reaction between Bz_2SnCl_2 and H_2L in equimolar amounts was conducted in boiling acetonitrile for 3 h to attempt the synthesis of [Bz_2Sn(L)] **4**. After evaporating the solvent, a crude material was obtained. When this crude product was dissolved in chloroform and repeatedly crystallized through heating and filtering, a small quantity of yellow crystals of [Sn(L)Cl_2] **9** was produced. During the crystallization, a possible facile double cleavage of the Sn-C bonds in the benzyl groups likely occurred due to the presence of incidental moisture, leading to the release of toluene and the formation of compound **9**, which contains two labile Cl atoms [43]. It is worth noting that attempts to isolate a larger quantity of the product were unsuccessful, preventing further spectroscopic studies. Nevertheless, melting point and diffraction studies were performed on the isolated yellow crystals, confirming a composition of [Sn(L)Cl_2]·$CHCl_3$. The purity of compounds **1**–**8** in bulk was established using ^{1}H, ^{13}C, and ^{119}Sn NMR analyses, with additional confirmation provided by HRMS results in acetonitrile. However, due to the limited number of available crystals and the insolubility of compound **9** in acetonitrile, NMR and HRMS analyses for this compound could not be carried out. To tackle the complex task of predicting the role of tin cations in the structures and the adaptability of flexible pentadentate ligands to various axial ligands, we focused on growing single crystals of the compounds. These crystals were subsequently analyzed using single-crystal X-ray diffraction, which definitively confirmed the formation of the molecular complexes (see X-ray discussion, *vide infra*).

Compounds **1**, and **5**–**9** are pale yellow solids, whereas compounds **2**–**4** are orange solids. They appear to be stable in both solid form and in solution.

The Experimental section includes a complete set of FT-IR spectra (refer to ESI Figs. S1-S10). The IR spectrum of H_2L displayed characteristic bands at approximately 3186, 2929, 1664, 1603, and 1567 cm^{-1}, corresponding to ν(NH), $\nu(C{-}H)_{aliphatic}$, $\nu(C{=}O)_{amide/keto}$, $\nu(C{=}N)_{imine}$, and $\nu(C{=}N)_{py}$, respectively. The absence of ν(NH) and ν(C═O) vibrations in compounds **1**–**9** indicates that the planar pentadentate ligand is bisdeprotonated, resulting in enolization of the amide carbonyl oxygen. Furthermore, the imino stretching frequencies ν(C═N) for the coordinated ligand were observed in the range of 1584 to 1598 cm^{-1}, while ν(C═N) for the pyridine was noted at around 1550 cm^{-1}. This confirms coordination by both the imino nitrogen atoms and the nitrogen atom of the pyridine ring [44]. Compounds **7** and **8** deserve special mention. In addition to the vibrations of a fully deprotonated ligand coordinated to a Sn atom, the IR spectrum of organotin(IV) compound **7** shows a prominent band at 2068 cm^{-1}, assigned to ν(N═N═N), indicating the presence of azide [45]. Additionally, the IR spectrum of compound **8** exhibited a relatively strong, sharp band at 2070 cm^{-1}, corresponding to the ν(NC) vibration of the NCS^- ion. The band associated with the ν(C-S) stretching frequency appears at 874 cm^{-1}. Therefore, the IR results suggest that **8** is an isothiocyanato complex, as indicated by the presence of N-bonded NCS, rather than a thiocyanato complex [46]. The structures of **7** and **8** were subsequently confirmed by diffraction studies (*vide infra*). The ^1H and ^{13}C NMR spectral data for compounds **1**–**8** are consistent with the proposed structure. In the $^1H/^{13}C$ NMR spectra of compounds **1**–**8** in $CDCl_3$, the pentadentate ligand shows generally little change upon coordination to the tin atom (ESI Figs. S11-S27). In general, only one set of signals is evident in the ^1H and ^{13}C NMR spectra of **1**–**9**, despite the presence of two arms in the ligand, implying that C_{2v} symmetry is preserved in solution. In DMSO-d_6 solvent, the ^1H NMR spectrum of H_2L shows a broad singlet at 10.8 ppm, corresponding to the amide NH (H-8) protons. Absence of the amide NH (H-8) signal in compounds **1**–**9** confirms the doubly deprotonated state of the ligand L^{2-}, likely due to amide-iminol tautomerism [31]. The $^2J(^{119}Sn,^1H)$, which is 116 Hz, is greater than those found in six-coordinated dimethyltin compounds [47] and seems to be typical of seven-coordinated species [48]. A sharp singlet in the range of 2.4 to 2.9 ppm, attributed to methyl groups, was also observed in the ^1H NMR spectra, alongside other ligand protons. In the ^{13}C NMR spectra of compounds **1**–**9**, the carbonyl carbon (C-9) resonates in the range of 168.0–173.4 ppm, while the C═N carbons (C-2 and C-5) resonate between 144.7–149.7 ppm and 143.5–146.0 ppm, respectively. However, bonding information from the chemical shifts could not be determined due to the use of two different solvents (H_2L in DMSO-d_6 for H_2L and $CDCl_3$ for **1**–**9**) for the NMR analysis. The ligand methyl carbon signal appeared at approximately 13 ppm. Aside from these observations, the $^1H/^{13}C$ NMR signals from Sn-R were found in the expected positions where they typically appear. Diorganotin(IV) compounds **1**–**3** exhibited sharp tin NMR signals in the range of −433.8 to −440.2 ppm (ESI Figs. 28–30), which aligns with observations for other structurally related organotin(IV) compounds containing the N_3O_2-chelating ligand [30,31,49]. Due to the presence of the N_3O_2-chelating ligand (L), the central tin atom in compounds **1**–**3** can be considered seven-coordinate with a distorted pentagonal bipyramidal geometry. The tin resonance in the dibenzyltin compound **4** showed a sharp singlet at −491.4 ppm (ESI Fig. 31), which is significantly shifted upfield relative to the corresponding [$R_2Sn(L)$] complexes (R = Me in **1**; *n*-Bu in **2**; and *n*-Oct in **3**), consistent with the literature [31]. In contrast, the monoorganohalo compounds **5** (R = *n*-Bu/Cl), **6** (*R* = Ph/Cl), azido compound **7** (R = *n*-Bu/N_3), and isothiocyanato compound **8** (R = *n*-Bu/NCS) exhibited even greater upfield shifts in the tin signals at −565.7, −612.2, −558.6, and −599.1 ppm (ESI Figs. 32–35), respectively. These shifts are likely due to the increased acidity from electronegative substituents. Thus, the tin NMR data for complexes **1**–**8** suggest that the central tin atom remains seven-coordinate in all cases.

The mass-to-charge ratios of the ions for H_2L and tin compounds **1**–**8** (ESI Figs. S36-S44) were measured in acetonitrile solution using high-resolution mass spectrometry. The mass spectra of the pro-ligand and organotin compounds **1**–**6** displayed a prominent monocharged ion, corresponding to a protonated molecule $[M + H]^+$. In contrast, the MS spectral patterns of azido compound **7** and isothiocyanato compound **8** revealed $[M\text{-}N_3]^+$ / $[M\text{-}NCS]^+$ as the main peak (100 % intensity), featuring a characteristic isotopic tin cluster in the positive ion mode as a result of the disconnection of the azido and isothiocyanato bonds [50]. These results are consistent with the calculated isotopic distribution of tin in acetonitrile solution (refer to experimental), indicating that compounds **1**–**6** remain stable in solution under high-energy electrospray conditions.

3.2. Description of the solid-state structures

The structures of compounds **1**–**9** were determined by low-temperature single-crystal X-ray diffraction. Crystallographic data and structure refinement statistics are given in Table S1. The compounds each feature a central Sn(IV) atom with an equatorially bound pentadentate L^{2-} ligand acting as a κ-N^3O^2 donor, with axial groups that are either purely organic (**1** = 2Me; **2** = 2*n*-Bu; **3** = 2*n*-Oct; **4** = 2Bz), organic/halide (**5** = *n*-Bu/Cl; **6** = Ph/Cl), organic/pseudohalide (**7** = *n*-Bu/N_3; **8** = *n*-Bu/NCS), or dihalide (**9** = 2Cl). Thus, the overall geometry about the Sn(IV) center in all cases is distorted pentagonal bipyramidal, with the degree of distortion dependent on the type of axial groups. Bond lengths and angles about the Sn(IV) centres are given in Tables 1 and 2, and a least-squares overlay plot of the central cores of the nine structures (Fig. 1) highlights the similarities. Although the geometries are similar, there are systematic differences in some bonding parameters across the structures. For example, the Sn-O bond lengths (Table 1) are significantly longer in **1**–**4** (average = 2.2618 Å) versus **5**–**8** (average = 2.1442 Å) and **9** (2.1168 Å). Similar trends are also apparent in the Sn-N bond distances. The perpendicular distance of the Sn atom from the mean plane through the κ-N^3O^2 bonding atoms (Table 1) indicates that when both axial groups are the same (structures **1**–**4**, and **9**), the Sn is close to coplanar with the κ-N^3O^2 bonding atoms (out-of-plane deviation range 0.0042–0.0305 Å, average 0.0138 Å), but when they are different (structures **5**–**8**), the Sn is markedly out of plane (deviation range 0.1393–0.2098 Å, average 0.1754 Å). These axial-group dependent differences provide a convenient means of grouping of the structures, thereby simplifying the following descriptions.

The molecular structures of **1**–**4** are shown in Fig. 2. The symmetry of crystals of **1**–**4** are all related, i.e., monoclinic $P2_1/c$ (**1, 4**) and $P2_1/n$ (**2, 3**), which are merely different settings of the same type of space group. Their unit cell parameters, however, are quite different (Table S1) and there are no consequential similarities between the crystal structures. Deviations from ideal (i.e., 180°) for the axial substituents relative to the Sn centre range from 169.15(6)° in **3** to 177.64(8)° in **2**, but there is no obvious correlation with the chemical nature or steric bulk of the axial substituents. The main differences in the molecular structures of **1**–**4**, aside from the nature of the axial organic groups are the torsions of the phenyl rings (Ph1 = C2-C7 and Ph2 = C18-C23) relative to their attached metallocycle (M1 = Sn1,O1,C1,N1,N2 and M2 = Sn1,O2,C17, N5,N4). These range from 0.99(8)° (i.e., almost coplanar) for the dihedral angle between M1 and Ph1 in **2** to 32.88(13)° between M1 and Ph1 in **1**. Full details are given in Table 2. Intermolecular contacts in **1**–**4** are mainly of the van der Waals type. There are no strong hydrogen bonds or π…π-stacking interactions in any of **1**–**4**. In **3**, however, a pair of weak contacts (C13-H13…O1^{sym} and C12-H12-O2^{sym}, *sym* = *-x* + 1, *y* - 1/2, *-z* + 3/2) join screw-related molecules into chains running parallel to the *b*-axis (Fig. 3). Packing plots viewed down each of the crystallographic axes for **1**–**4** are given in Figs. S45-S56.

The molecular structures of **5**–**8** are shown in Fig. 4. These mixed axial-ligand crystal structures exhibit a range of space-group symmetries. Crystals of **5** have space-group type $P2_1/n$, those of **6** have space-

Table 1
Selected distances (Å) in compounds 1–9.

distance	1	2	3	4	5
Sn-L_{NO}	0.0056(11)	0.0042(7)	0.0082(5)	0.0205(6)	0.1393(6)
Sn1-O1	2.273(2)	2.2246(12)	2.2756(9)	2.2803(12)	2.1629(11)
Sn1-O2	2.273(2)	2.2469(13)	2.2945(9)	2.2261(13)	2.1458(11)
Sn1-N2	2.335(2)	2.3530(16)	2.3401(11)	2.3460(15)	2.2766(14)
Sn1-N3	2.377(2)	2.3663(16)	2.3462(11)	2.3473(14)	2.3041(13)
Sn1-N4	2.334(2)	2.3336(15)	2.3626(11)	2.3116(15)	2.2819(13)
Sn1-C24	2.123(3)	2.1437(18)	2.1405(14)	2.1782(18)	2.1861(16)[b]
Sn1-C25	2.119(3)	2.146(2)[b]	2.1374(13)	2.1633(18)	–
C1-O1	1.277(4)	1.281(2)	1.2814(15)	1.271(2)	1.2892(19)
C17-O2	1.284(4)	1.282(2)	1.2773(15)	1.281(2)	1.2933(19)
N1-N2	1.376(3)	1.380(2)	1.3760(16)	1.379(2)	1.3700(19)
N4-N5	1.373(3)	1.375(2)	1.3732(15)	1.370(2)	1.3740(18)
6	**7**	**8**	**9**[a]		
0.1800(8)	0.1724(8)	0.2098(7)	0.0305(8)		
2.1405(17)	2.1562(16)	2.1521(12)	2.1168(11)		
2.1339(17)	2.1282(16)	2.1337(12)	–		
2.263(2)	2.292(2)	2.2763(15)	2.2441(13)		
2.2843(19)	2.3064(19)	2.3101(14)	2.2561(19)		
2.280(2)	2.284(2)	2.2686(15)	–		
2.157(2)	2.143(2)	2.140(4)[b]	–		
–	–	–	–		
1.290(3)	1.285(3)	1.285(2)	1.2985(19)		
1.293(3)	1.290(3)	1.289(2)	–		
1.377(3)	1.381(3)	1.371(2)	1.3706(18)		
1.377(3)	1.369(3)	1.3741(18)	–		

a Missing entries in **9** are equivalent by mirror symmetry.
b Major component of disorder only.
L_{NO} refers to the mean plane through L^{2-} coordinating N and O atoms.

Table 2
Selected angles (°) in compounds 1–9.

angle	1	2	3	4	5
O1-Sn1-O2	89.06(7)	88.65(4)	89.65(3)	88.57(5)	81.34(4)
O1-Sn1-N2	68.52(8)	68.55(5)	68.13(4)	68.00(5)	70.33(5)
O2-Sn1-N4	68.57(8)	68.71(5)	67.26(4)	69.04(5)	70.60(4)
N2-Sn1-N3	67.00(9)	66.95(5)	67.62(4)	66.98(5)	68.67(5)
N3-Sn1-N4	66.89(9)	67.30(6)	67.38(4)	67.70(5)	68.28(5)
R_{ax}-Sn1-R_{ax}'	175.44(12)	177.64(8)[b]	169.15(6)	173.44(7)	179.15(7)[b]
O1-C1-C2-C3	30.8(4)	0.1(3)	12.15(18)	16.1(2)	3.2(2)
O2-C17-C18-C19	17.6(5)	5.7(3)	7.54(18)	13.1(3)	7.9(2)
∠ L_{M1}-L_{Ph1}	32.88(13)	0.99(8)	11.76(8)	20.14(8)	4.07(11)
∠ L_{M2}-L_{Ph2}	18.72(16)	12.40(9)	9.63(7)	16.25(8)	8.35(8)
∠ L_{NO}-L_{NR}	89.33(6)	87.46(4)	88.39(3)	89.42(5)	89.78(4)
6	**7**	**8**	**9**[a]		
79.15(7)	81.82(6)	80.81(5)	78.07(6)[c]		
70.94(7)	69.97(6)	70.19(5)	71.43(4)		
70.62(7)	70.84(6)	70.93(5)	–		
69.27(7)	68.19(7)	67.91(5)	69.53(3)		
68.71(7)	68.01(7)	68.37(5)	–		
177.63(7)	176.04(9)	175.6(2)[b]	176.32(2)		
17.7(4)	0.0(3)	11.8(3)	3.2(2)		
10.2(4)	8.9(3)	1.4(3)	–		
21.51(12)	6.65(14)	13.34(10)	10.39(9)		
11.36(11)	9.26(12)	4.17(9)	–		
88.89(6)	88.25(6)	86.35(13)	90.000(2)		

a Missing entries for **9** have equivalents by crystallographic mirror symmetry.
b Major component of disorder only.
c This angle is O1-Sn1-O1^{m} ($m = x$, 0.5-y, z).
R_{ax} and $R_{ax'}$ represent the axial-group atoms attached to Sn1.
L_{M1} and L_{M2} are the mean planes of metallocycles Sn1-O1-C1-N1-N2 and Sn1-O2-C17-N5-N4.
L_{Ph1} and L_{Ph2} are the mean planes of phenyl rings C2-C3-C4-C5-C6-C7 and C18-C19-C20-C21-C22-C23.
L_{NO} is the mean plane through L^{2-} atoms O1,N2,N3,N4,O2 coordinating to Sn1.
L_{NR} is the mean plane through L^{2-} atom N3 and the axial atoms attached to Sn1.

group type $P2_12_12_1$ (the only Sohncke space group for any of **1**–**9**), but the crystals are twinned by inversion. Both **7** and **8** are trigonal, space-group type $R\bar{3}$. Structure **5** has disorder of its axial *n*-Bu group and includes a toluene solvent molecule statistically disordered about a crystallographic inversion centre. The molecules loosely stack into columns parallel to the *a*-axis, which in turn creates solvent-accessible channels (also parallel to the *a*-axis), which are occupied by the disordered toluene (Fig. S57). Structure **6** is not disordered and is solvent free. The unit cell parameters of **7** and **8** are similar (Table S1), suggesting similarity in overall packing (Fig. 5), but there are no obvious similarities

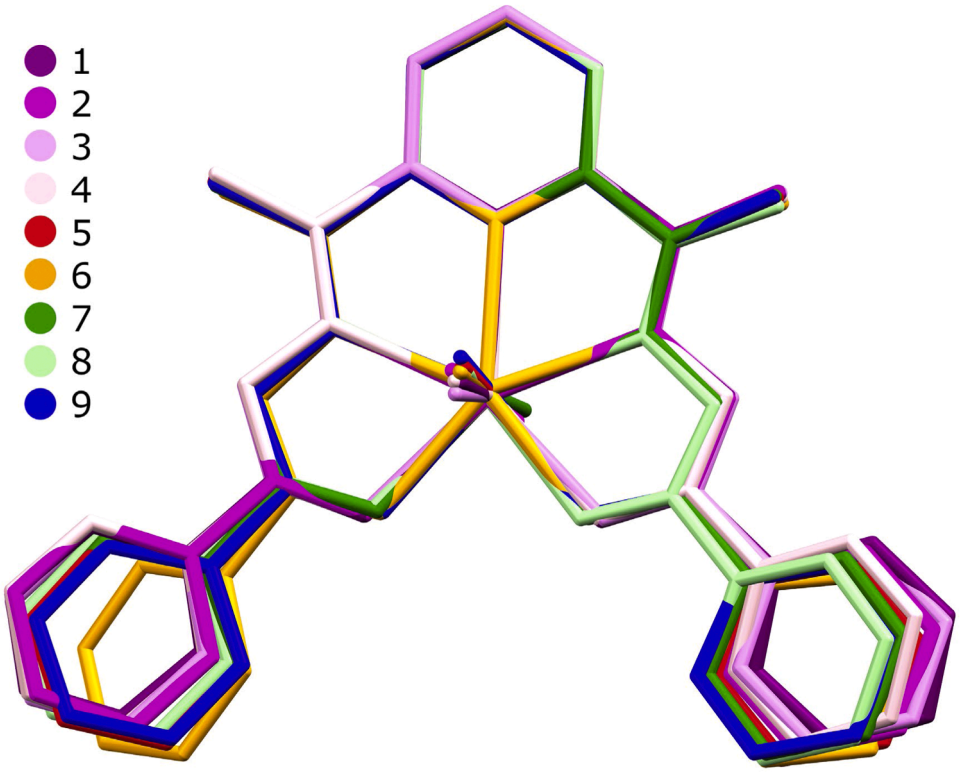

Fig. 1. A least-squares overlay plot (fit through O1, O2, N2, N3, N4, and Sn1) for each of compounds **1**–**9**. Axial groups attached to Sn1 were truncated at the first atom. The main differences are the torsions of the pendant phenyl rings.

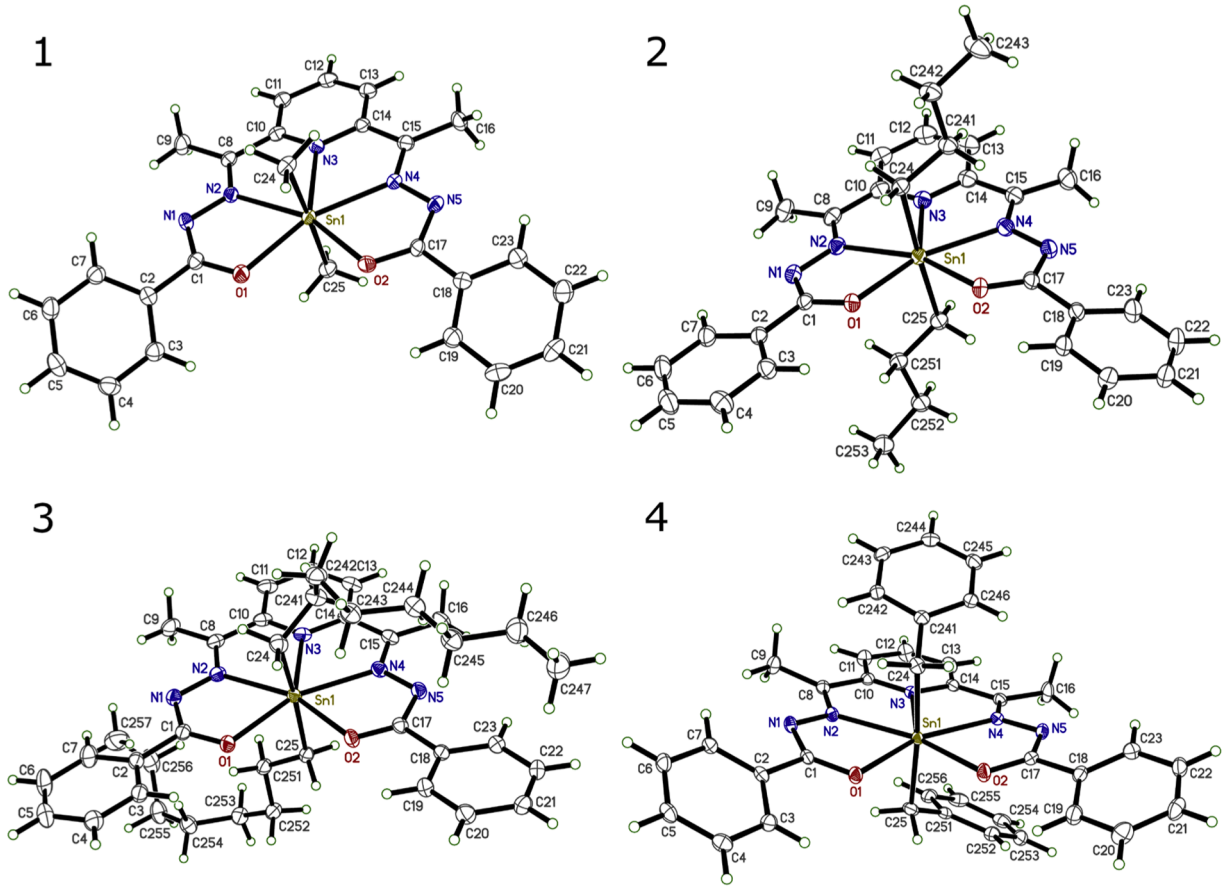

Fig. 2. Ellipsoid plots (50 % probability) of compounds **1**–**4**. Minor *n*-Bu disorder (~8 % occupancy) in compound **2** is omitted for the sake of clarity.

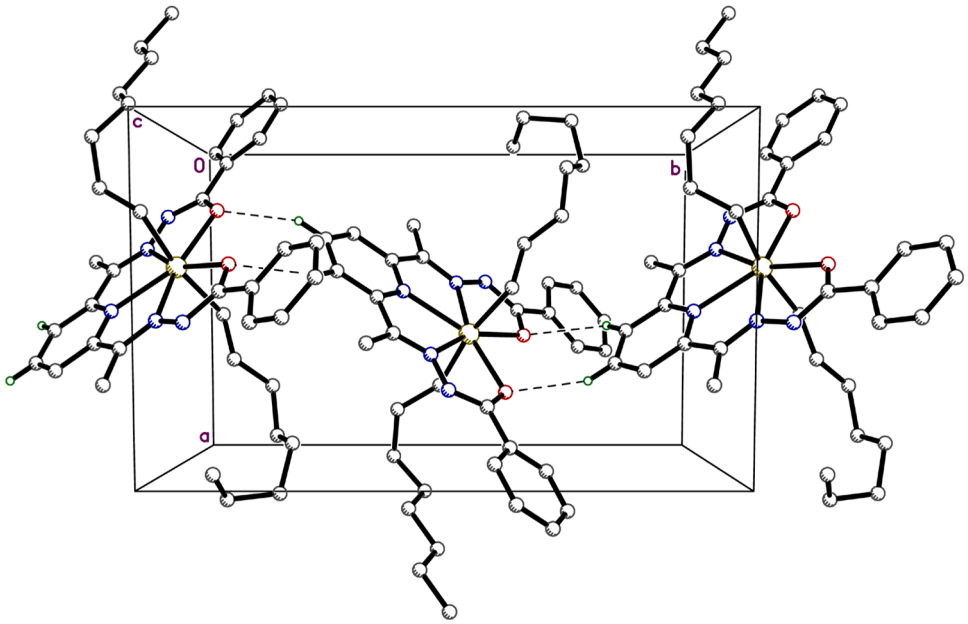

Fig. 3. A partial packing plot of compound **3** viewed down the crystallographic *c*-axis, showing chains of molecules extending parallel to the *b*-axis formed by pairs of weak C—H…O interactions (dashed lines).

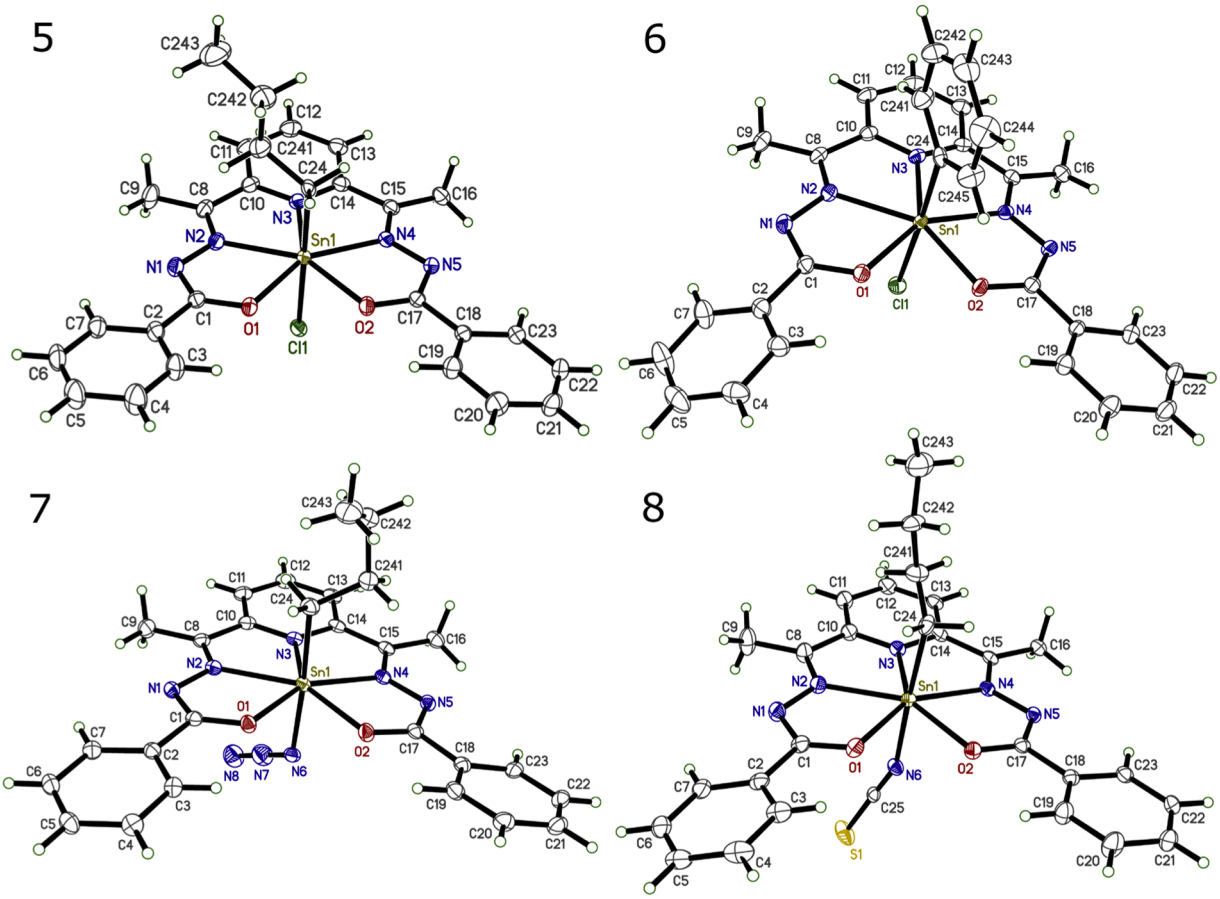

Fig. 4. Ellipsoid plots (50 % probability for **5** and **6**, 30 % for **7** and **8**) of compounds **5**–**8**. In **5**, a toluene solvent molecule disordered about a crystallographic inversion centre is omitted to enhance the clarity. Similarly, minor components of disorder in **5** (*n*-Bu, ~6.5 %) and **8** (*n*-Bu, two minor components of ~27 % and 22 %; NCS, ~11 %) are omitted for the sake of clarity.

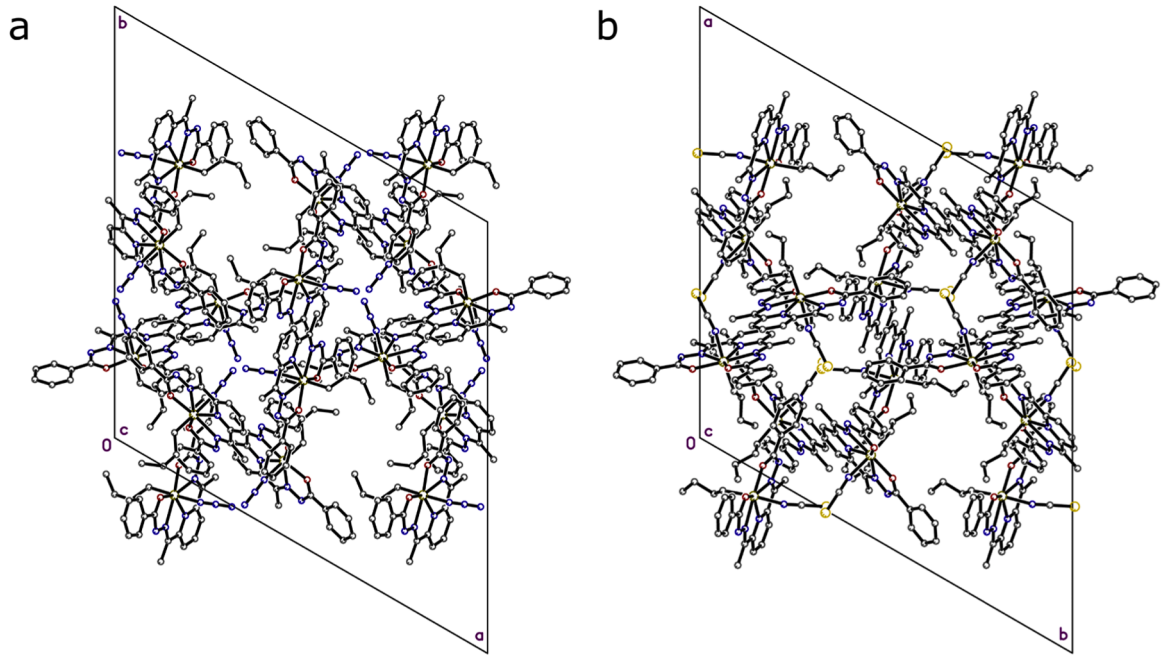

Fig. 5. Packing plots of (a) **7** and (b) **8** viewed down their crystallographic *c*-axes. Similar solvent accessible channels are present in both structures.

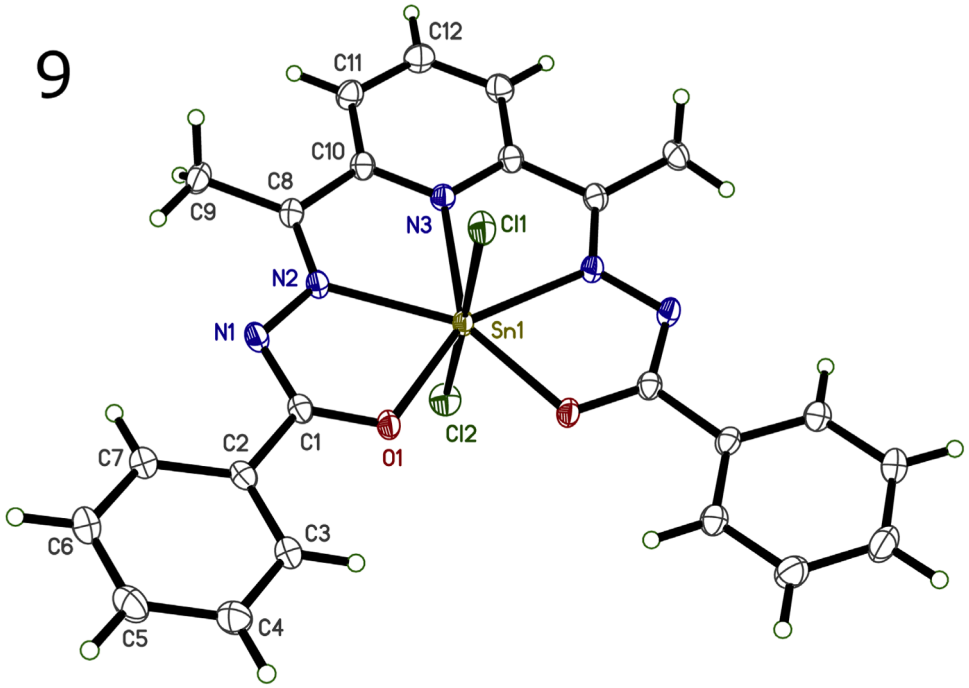

Fig. 6. An ellipsoid plot (50 % probability) of compound **9**. The molecule straddles a crystallographic mirror plane, so only half the atoms are labeled. A chloroform solvent molecule has been omitted for the sake of clarity.

with either **5** or **6**. In both **7** and **8**, molecules form loose columnar stacks parallel to the *c*-axis that generate solvent- accessible channels that also run parallel to the *c*-axis, which are evident in Fig. 5. The contents of these channels were extensively disordered; attempts to model chemically reasonable fragments were unsuccessful and so were removed using *SQUEEZE* [42]. Aside from the solvent channels, structure **7** is not disordered, whereas **8** shows extensive disorder of both its *n*-Bu axial group (three disorder components modelled major ~50.5 %; minor 27 % and 22.5 %) and the NCS axial group (two components, ~89 % and 11 %). In **7**, there is a weak contact between H11 of the L ligand and azide N8 of an adjacent (distance = 2.47 Å, via -*y* + 2/3, x-*y* + 1/3, *z* + 1/3) molecule. Structure **8** has weak contacts involving H9C and H11 to the thiocyanate S1, but the distances are longer (~2.81–2.99 Å) and the interactions are less distinct due to disorder. Similar to **1**–**4**, there are no strong H-bonds or π…π-stacking interactions in **5**–**8**, intermolecular contacts are mainly van der Waals-type interactions.

The molecular structure of the dichloro compound, **9**, is shown in Fig. 6. The crystals have space-group type *Pnma* in which the molecule straddles the mirror plane, thus *Z*' (the number of formula units per asymmetric unit) is 0.5. This contrasts with **1**–**8**, where *Z*' = 1. There are

no disordered atoms in **9**, but there is a solvent chloroform molecule, which also lies on the mirror plane. It forms weak bifurcated hydrogen bonds of the form C1S-H1S…O1 = 3.456(3)Å (and to $O1^{sym}$, *sym* = *x*, 1/2 - *y*, *z*). The overall packing generates solvent-accessible channels parallel to the *a*-axis, occupied by the chloroform solvent (Fig. S68). As with **1**–**8**, there are no strong H-bonds. Generic packing plots for **1**–**9** viewed down each crystallographic axis are given in the supplementary information (ESI Fig. S45–70).

4. Conclusions

In conclusion, this study highlights the significant progress made in synthesizing and characterizing a variety of stable tin(IV) complexes using the 2,6-diacetylpyridine bis(benzoylhydrazone) pro-ligands (H_2L). These complexes exhibit robust coordination chemistry, with the ligand acting as a κ-N_3O_2 donor and different axial ligands, resulting in a seven-coordinate, distorted pentagonal bipyramidal geometry around the tin center. The study systematically explores the effect of different axial ligands, such as alkyl groups (Me, *n*-Bu, *n*-Oct, Bz), chloride (Cl), azido (N_3), and isothiocyanato (NCS) ligands, on the overall structure and stability of the complexes. X-ray diffraction analysis of the synthesized compounds confirms the asymmetrical arrangement of the two arms of the pentadentate L^{2-} ligand, which is crucial in determining the steric and electronic properties of the resulting tin complexes. The steric influence of larger axial ligands, such as *n*-Oct and Bz, is particularly noteworthy, as they introduce significant strain into the complex, potentially causing greater distortion of the SnN_3O_2 coordination geometry. Additionally, the substitution of halide ligands with more electron-rich species, such as N_3 or NCS, alters the electronic environment of the tin(IV) center, influencing both the stability and reactivity of the complexes. These electronic and steric factors play a crucial role in determining the behavior of the complexes, which is confirmed through various spectroscopic techniques, including ^{1}H, ^{13}C, and ^{119}Sn NMR, as well as HRMS. The ^{119}Sn NMR spectra reveal typical chemical shifts associated with hypercoordinated tin, ranging from −433 to −628 ppm, indicating strong coordination and shielding of the central tin atom. Both NMR and HRMS, and X-ray further confirm the monomeric nature and stable composition of the complexes both in solution and in solid-state forms, highlighting their potential for consistent synthesis and applications. Considering the potential applications of these tin(IV) complexes, future studies could aim to improve their catalytic activity and stability by manipulating axial ligands, thus paving the way for their use in a variety of catalytic processes. Furthermore, the unique properties of these complexes could be exploited in materials science, particularly in the development of materials with tailored electronic, magnetic, or optical properties. Additionally, their biological potential, including anticancer and antimicrobial effects, may offer an exciting opportunity for therapeutic research.

CRediT authorship contribution statement

Tushar S. Basu Baul: Writing – review & editing, Writing – original draft, Supervision, Resources, Project administration, Investigation, Funding acquisition, Formal analysis, Conceptualization. **Avishek Khatiwara:** Validation, Software, Methodology, Investigation, Data curation. **Amon Das:** Validation, Methodology, Investigation. **Andrew Duthie:** Writing – review & editing, Validation, Methodology, Investigation, Formal analysis, Data curation. **Sean Parkin:** Writing – review & editing, Validation, Software, Resources, Investigation, Funding acquisition, Formal analysis, Data curation.

Declaration of competing interest

The authors declare that they have no conflicts of interest regarding the publications of this paper.

Acknowledgements

AK and AD thank University Grants Commission, New Delhi for the award of non-NET fellowships. Authors (TSBB, AK and AD) thank SAIF-NEHU, Shillong for providing NMR measurements and the DST-FIST program (No. SR/FST/CS-II/2019/99(C)), Government of India, for providing the HRMS instrument to the Department of Chemistry, NEHU, Shillong. Deakin University's Advanced Characterization Facility is acknowledged for use of the NMR instrumentation. SP thanks the US NSF MRI program (grant CHE-1625732).

Supplementary materials

Supplementary material associated with this article can be found, in the online version, at doi:10.1016/j.molstruc.2025.142137.

Data availability

Data will be made available on request.

References

[1] P. Das, W. Linert, Schiff base-derived homogeneous and heterogeneous palladium catalysts for the Suzuki-Miyaura reaction, Coord. Chem. Rev 311 (2016) 1–23.
[2] X. Liu, C. Manzur, N. Novoa, S. Celedón, D. Carrillo, J.-R. Hamon, Multidentate unsymmetrically-substituted Schiff bases and their metal complexes: synthesis, functional materials properties, and applications to catalysis, Coord. Chem. Rev 357 (2018) 144–172.
[3] D.J. Harding, P. Harding, W. Phonsri, Spin crossover in iron(III) complexes, Coord. Chem. Rev 313 (2016) 38–61.
[4] P. Gütlich, Y. Garcia, H.A. Goodwin, Spin crossover phenomena in Fe(II) complexes, Chem. Soc. Rev 29 (2000) 419–427.
[5] L. Pogány, B. Brachňaková, J. Moncol, J. Pavlik, I. Nemec, Z. Trávníček, M. Mazúr, L. Bučinský, L. Suchánek, I. Šalitroš, Impact of substituent variation on the presence of thermal spin crossover in a series of mononuclear iron(III) Schiff base complexes with terminal pseudohalido co-ligands, Chem. Eur. J. 24 (2018) 5191–5203.
[6] X. Liu, J.-R. Hamon, Recent developments in penta-, hexa- and heptadentate Schiff base ligands and their metal complexes, Coord. Chem. Rev 389 (2019) 94–118.
[7] M.M. Radanović, B.B. Holló, Some aromatic schiff bases and their metal complexes. Schiff base in organic, inorganic and physical chemistry, IntechOpen (2023), https://doi.org/10.5772/intechopen.107405.
[8] L.D. Popov, A.N. Morozov, I.N. Shcherbakov, Y.P. Tupolova, V.V. Lukov, V. A. Kogan, Metal complexes with polyfunctional ligands based of bis(hydrazones) of dicarbonyl compounds, Russ. Chem. Rev 78 (2009) 643–658.
[9] I. Ivanović-Burmazović, K. Andjelković, Transition metal complexes with bis (hydrazone)ligands of 2,6-diacetylpyridine. Hepta-coordination of 3d metals, Adv. Inorg. Chem 55 (2004) 315–360.
[10] (a) A.K. Bar, N. Gogoi, C. Pichon, V.M.L.D.P. Goli, M. Thlijeni, C. Duhayon, N. Suaud, N. Guihéry, A.-L. Barra, S. Ramasesha, J.-P. Shutter, Pentagonal bipyramid FeII complexes: robust ising-spin units towards heteropolymer nanomagnets, Chem. Eur.J. 23 (2017) 4380–4396;
(b) A.K. Bar, P. Kalita, J.-P. Sutter, V. Chandrasekhar, Pentagonal-bipyramid ln (III) complexes exhibiting single-ion-magnet behavior: a rational synthetic approach for a rigid equatorial plane, Inorg. Chem. 57 (2018) 2398–2401;
(c) V.D. Sasnovskaya, V.A. Kopotkov, A.V. Kazakova, A.D. Talantsev, R. B. Morgunov, S.V. Simonov, L.V. Zorina, V.S. Mironov, E.B. Yagubskii, Slow magnetic relaxation in mononuclear complexes of Tb, Dy, Ho and Er with the pentadentate (N_3O_2) Schiff-base dapsc ligand, New J. Chem 42 (2018) 14883–14893;
(d) A.K. Mondal, A. Mondal, B. Dey, S. Konar, Influence of the coordination environment on easy-plane magnetic anisotropy of pentagonal bipyramidal Cobalt (II) complexes, Inorg. Chem 57 (2018) 9999–10008;
(e) V.A. Kopotkov, D.V. Korchagin, V.D. Sasnovskaya, I.F. Gilmutdinov, E. B. Yagubskii, A series of field-induced single-ion magnets based on the seven-coordinate Co(II) complexes with the pentadentate (N_3O_2) H_2dapsc ligand, Magnetochemistry 5 (2019) 58.
[11] (a) N. Gogoi, M. Thlijeni, C. Duhayon, J.-P. Sutter, Heptacoordinated nickel(II) as an ising-type anisotropic building unit: illustration with a pentanuclear [$(NiL)_3${$W(CN)_8$}$_2$] complex, Inorg. Chem. 52 (2013) 2283–2285;
(b) V.D. Sasnovskaya, V.A. Kopotkov, A.D. Talantsev, R.B. Morgunov, E. B. Yagubskii, S.V. Simonov, L.V. Zorina, V.S. Mironov, Synthesis, structure, and magnetic properties of 1D {[$Mn^{III}(CN)_6$][Mn^{II}(dapsc)]}$_n$ coordination polymers: origin of unconventional single-chain magnet behavior, Inorg. Chem. 56 (2017) 8926–8943;
(c) C. Pichon, N. Suaud, C. Duhayon, N. Guihéry, J.-P. Sutter, Cyano-bridged Fe (II)-Cr(III) single-chain magnet based on pentagonal bipyramid units: on the added value of aligned axial anisotropy, J. Am. Chem. Soc. 140 (2018) 7698–7704;
(d) L.V. Zorina, S.V. Simonov, V.D. Sasnovskaya, A.D. Talantsev, R.B. Morgunov,

V.S. Mironov, E.B. Yagubskii, Slow magnetic relaxation, antiferromagnetic ordering, and metamagnetism in $Mn^{II}(H_2dapsc)$-$Fe^{III}(CN)_6$ chain complex with highly anisotropic Fe-CN-Mn spin coupling, Chem. Eur. J. 25 (2019) 14583–14597;
(e) J.-H. Wang, Z.-Y. Li, M. Yamashita, X.-H. Bu, Recent progress on cyano-bridged transition-metal-based single-molecule magnets and single-chain magnets, Coord. Chem. Rev. 428 (2021) 213617.

[12] (a) A. Dey, P. Kalita, V. Chandrasekhar, Lanthanide(III)-based single-ion magnets, ACS Omega 3 (2018) 9462–9475;
(b) P. Kalita, N. Ahmed, A.K. Bar, S. Dey, A. Jana, G. Rajaraman, J.-P. Sutter, V. Chandrasekhar, Pentagonal bipyramidal Ln(III) complexes containing an axial phosphine oxide ligand: field-induced single-ion magnetism behavior of the Dy(III) analogues, Inorg. Chem 59 (2020) 6603–6612;
(c) G. Peng, Y. Chena, B. Li, One-dimensional lanthanide coordination polymers supported by pentadentate Schiff-baseand diphenyl phosphate ligands: single molecule magnet behavior and photoluminescence, New J. Chem 44 (2020) 7270–7276;
(d) M.A. Fik-Jaskółka, I. Pospieszna-Markiewicz, G.N. Roviello, M. Kubicki, W. Radecka-Paryzek, V. Patroniak, Synthesis and spectroscopic investigation of a hexaaza lanthanum(III) macrocycle with a hybrid-type G4 DNA stabilizing effect, Inorg. Chem 60 (2021) 2122–2126;
(e) T.A. Bazhenova, V.A. Kopotkov, D.V. Korchagin, Y.V. Manakin, L.V. Zorina, S. V. Simonov, I.A. Yakushev, V.S. Mironov, A.N. Vasiliev, O.V. Maximova, E. B. Yagubskii, A series of novel pentagonal-bipyramidal erbium(III) complexes with acyclic chelating N_3O_2 Schiff-base ligands: synthesis, structure, and magnetism, Molecules 26 (2021) 6908;
(f) L. Spillecke, C. Koo, O. Maximova, V.S. Mironov, V.A. Kopotkov, D. V. Korchagin, A.N. Vasiliev, E.B. Yagubskii. R. Klingeler, Magnetic behavior of the novel pentagonal bipyramidal erbium(III) complex (Et_3NH) $[Er(H_2DAPS)Cl_2]$: high-frequency EPR study and crystal-field analysis, Dalton Trans 50 (2021) 18143–18154;
(g) V. Singh, D. Das, S. Anga, J.-P. Sutter, V. Chandrasekhar, A.K. Bar, Rigid N_3O_2pentadentate ligand-assisted octacoordinate mononuclear ln(III) complexes: syntheses, Characterization, and Slow Magnetization Relaxation ACS Omega 7 (2022) 25881–25890;
(h) H.-Q. Li, Y.-C. Sun, L. Shi, F.-L. Chen, F.-X. Shen, Y. Zhao, X.-Y. Wang, Inorg. Chem 61 (2022) 2272–2283;
(i) P. Kalita, N. Ahmed, S. Moorthy, V. Béreau, A.K. Bar, P. Kumar, P. Nayak, J.-P. Sutter, S.K. Singh, V. Chandrasekhar, Slow magnetic relaxation in a homoaxially phosphine oxide coordinated pentagonal bipyramidal Dy(III) complex, Dalton Trans 52 (2023) 2804–2815.

[13] Q. Yao, J. Qi, Y. Zheng, K. Qian, L. Wei, M. Maimaitiyiming, Z. Cheng, Y. Wang, Synthesis, anticancer activity and mechanism of iron chelator derived from 2,6-diacetylpyridine bis(acylhydrazones), J. Inorg. Biochem 193 (2019) 1–8.

[14] K. Anđelković, M.R. Milenković, A. Pevec, I. Turel, I.Z. Matić, M. Vujčić, D. Sladić, D. Radanović, G. Brađan, S. Belošević, B. Čobeljić, Synthesis, characterization and crystal structures of two pentagonal-bipyramidal Fe(III) complexes with dihydrazone of 2,6-diacetylpyridine and Girard's T reagent. Anticancer properties of various metal complexes of the same ligand, J. Inorg. Biochem 174 (2017) 137–149.

[15] K.S.O. Ferraz, N.F. Silva, J.G. da Silva, L.F. de Miranda, C.F.D. Romeiro, E. M. Souza-Fagundes, I.C. Mendes, H. Beraldo, Investigation on the pharmacological profile of 2,6-diacetylpyridine bis(benzoylhydrazone) derivatives and their antimony(III) and bismuth(III) complexes, Eur. J. Med. Chem 53 (2012) 98–106.

[16] G.F. Liu, M. Filipović, F.W. Heinemann, I. Ivanović-Burmazović, Seven-coordinate iron and manganese complexes with acyclic and rigid pentadentate chelates and their superoxide dismutase activity, Inorg. Chem 46 (2007) 8825–8835.

[17] C.T. Gutman, T.C. Brunold, Spectroscopic and computational studies of a small-molecule functional mimic of iron superoxide dismutase, iron 2,6-diacetylpyridinebis(semioxamazide), Inorg. Chem 51 (2012) 12729–12737.

[18] C.T. Gutman, I.A. Guzei, T.C. Brunold, Structural, spectroscopic, and computational characterization of the azide adduct of feiii(2,6-diacetylpyridinebis (semioxamazide)), a functional analogue of iron superoxide dismutase, Inorg. Chem 52 (2013) 8909–8918.

[19] M. Kozłowski, R. Kierzek, M. Kubicki, W. Radecka-Paryzek, Metal-promoted synthesis, characterization, crystal structure and RNA cleavage ability of 2,6-diacetylpyridine bis(2-aminobenzoylhydrazone) lanthanide complexes, J. Inorg. Biochem 126 (2013) 38–45.

[20] C. Gökçe, N. Dilek, R. Gup, Seven coordinated cobalt(II) complexes with 2,6-diacetylpyridine bis(4-acylhydrazone) ligands: synthesis, characterization, DNA-binding and nuclease activity, Inorg. Chim. Acta 432 (2015) 213–220.

[21] R. Gup, C. Gökçe, N. Dilek, Seven-coordinated cobalt(II) complexes with 2,6-diacetylpyridine bis(4-hydroxybenzoylhydrazone): synthesis, characterisation, DNA binding and cleavage properties, Supramol. Chem 27 (2015) 629–641.

[22] K. Nomiya, K. Sekino, M. Ishikawa, A. Honda, M. Yokoyama, N.C. Kasuga, H. Yokoyama, S. Nakano, K. Onodera, Syntheses, crystal structures and antimicrobial activities of monomeric 8-coordinate, and dimeric and monomeric 7-coordinate bismuth(III) complexes with tridentate and pentadentate thiosemicarbazones and pentadentate semicarbazone ligands, J. Inorg. Biochem 98 (2004) 601–615.

[23] P. Mazza, F. Zani, M. Orcesi, C. Pelizzi, G. Pelizzi, G. Predieri, Synthesis, structure, antimicrobial, and genotoxic activities of organotin compounds with 2,6-diacetylpyridine nicotinoyl- and isonicotinoylhydrazones, J. lnorg. Biochem 48 (1992) 251–270.

[24] N.C. Kasuga, K. Sekino, M. Ishikawa, A. Honda, M. Yokoyama, S. Nakano, N. Shimada, C. Koumo, K. Nomiya, Synthesis, structural characterization and antimicrobial activities of 12 zinc(II) complexes with four thiosemicarbazone and two semicarbazone ligands, J. Inorg. Biochem 96 (2003) 298–310.

[25] I. Czyżewska, L. Mazur, L. Popiołek, Transition metal complexes of hydrazones as potential antimicrobial and anticancer agents: a short review, Chem. Biol. Drug. Des 104 (2024) e14590.

[26] C. Pelizzi, G. Pelizzi, Investigation into aroylhydrazones as chelating agents. Synthesis and structural characterization of a tin(IV) complex with 2,6-diacetylpyridine bis(salicyloylhydrazone), J. Chem. Soc., Dalton Trans (1980) 1970–1973.

[27] C. Pelizzi, G. Pelizzi, G. Predieri, Investigation into aroylhydrazones as chelating agents: V. Synthesis and structural characterization of two seven-coordinate organotin(IV) complexes with 2,6-diacetylpyridine bis(2-aminobenzoylhydrazone), J. Organomet. Chem 263 (1984) 9–20.

[28] D. Delledonne, G. Pelizzi, C. Pelizzi, Structure of a seven-coordinated tin(IV)-hydrazone complex, Acta Crystallogr C43 (1987) 1502–1505.

[29] R. Pedrido, M.J. Romero, M.R. Bermejo, A.M. González-Noya, M. Maneiro, M. J. Rodríguez, G. Zaragoza, Influence of the metal size in the structure of the complexes derived from a pentadentate $[N_3O_2]$ hydrazone, Dalton Trans (2006) 5304–5314.

[30] M. Careri, A. Mangia, G. Predieri, C. Vignali, The ^{1}H, ^{13}C and ^{119}Sn NMR spectra of heptacoordinated diorganotin(IV) complexes, J. Organomet. Chem 375 (1989) 39–44.

[31] T.S. Basu Baul, B. Hlychho, S. Das Pramanik, A. Lyčka, P. Roy, A.G. Mahmoud, F. C M, Guedes da Silva, Organotin(IV) complexes derived from 2,6-diacetylpyridine bis (2-hydroxybenzoylhydrazone) as prospective anti-proliferative agents: synthesis, characterization, structures and in *vitro* anticancer activity, J. Inorg. Biochem 261 (2024) 112693.

[32] S. Parkin, H. Hope, Macromolecular cryocrystallography: cooling, mounting, storage and transportation of crystals, J. Appl. Crystallogr 31 (1998) 945–953.

[33] Bruker-AXS. *APEX5, SMART, SAINT*, Bruker AXS Inc, Madison, Wisconsin, USA, 2023.

[34] L. Krause, R. Herbst-Irmer, G.M. Sheldrick, D. Stalke, Comparison of silver and molybdenum microfocus x-ray sources for single-crystal structure determination, J. Appl. Crystallogr 48 (2015) 3–10.

[35] S. Parkin, B. Moezzi, H. Hope, XABS2: an empirical absorption correction program, J. Appl. Crystallogr 28 (1995) 53–56.

[36] G.M. Sheldrick, SHELXT-integrated space-group and crystal-structure determination, Acta Crystallogr A71 (2015) 3–8.

[37] G.M. Sheldrick, SHELXL-crystal structure refinement with SHELXL, Acta Crystallogr C71 (2015) 3–8.

[38] A.L. Spek, checkCIF validation ALERTS: what they mean and how to respond, Acta Crystallogr E76 (2015) 1–11.

[39] S. Parkin, Expansion of scalar validation criteria to three dimensions: the R-tensor, Acta Crystallogr A56 (2000) 157–162.

[40] S.R. Parkin, Practical hints and tips for solution of pseudo-merohedric twins: three case studies, Acta Crystallogr E77 (2021) 452–465.

[41] M. Sevvana, M. Ruf, I. Usón, G.M. Sheldrick, R. Herbst-Irmer, Non-merohedral twinning: from minerals to proteins, Acta Crystallogr D75 (2019) 1040–1050.

[42] A.L. Spek, Platon squeeze: a tool for the calculation of the disordered solvent contribution to the calculated structure factors, Acta Crystallogr C71 (2015) 9–18.

[43] T.S. Basu Baul, R. Manne, A. Duthie, L.Y. Liew, J. Chew, S.M. Lee, E.R.T. Tiekink, Synthesis, structural and in vitro biological evaluation of diamondoid-decorated lipophilic organotin(IV) derivatives, J. Organomet. Chem 941 (2021) 121802.

[44] X.S. Gao, X. Jiang, C. Yao, Two new complexes of lanthanide(III) ion with the N_3O_2-donor Schiff base ligand: synthesis, crystal structure, and magnetic properties, J. Mol. Struct 1126 (2016) 275–279.

[45] (a) P. Švec, K. Bartoš, Z. Růžičková, P. Cuřínovác, L. Dušek, J. Turek, F. De Proft, A. Růžička, C,N-chelated organotin(IV) azides: synthesis, structure and use within the click chemistry, New J. Chem 40 (2016) 5808–5817;
(b) G. Socrates. Infrared Characteristic Group Frequencies, John Wiley & Sons, Chichester, UK, 1980;
(c) K. Nakamoto. Infrared and Raman Spectra of Inorganic and Coordination Compounds, 3rd edn, John Wiley & Sons, New York, USA, 1978.

[46] (a) B.Z. Momeni, F. Shirvani, J. Janczak, Synthesis, structural characterization, Hirshfeld surface analysis, and thermal properties of dibutyltin(IV) complexes with thiocyanate and pyridyl ligands, J. Mol. Struct 1317 (2024) 139155;
(b) M. Wada, R. Okawara, Infrared spectra of alkyltin isothiocyanates, J. Organomet. Chem 8 (1967) 261–270.

[47] T.P. Lockhart, W.F. Manders, Structure determination by NMR spectroscopy. Correlation of $|^{2}J(^{119}Sn,^{1}H)|$ and the me-Sn-me angle in methyltin(IV) compounds, Inorg. Chem 25 (1986) 892–895.

[48] J. Otera, T. Hinoishi, R. Okawara, ^{119}Sn chemical shifts in seven-coordinate organotin compounds, J. Organomet. Chem 202 (1980) C93–C94.

[49] C. Carini, G. Pelizzi, P. Tarasconi, C. Pelizzi, K.C. Molloy, P.C. Waterfield, Synthesis, infrared, and tin-119 Mössbauer spectroscopic characterization of seven-coordinate diorganotin(IV) adducts with 2,6-diacetylpyridine acylhydrazones, including the X-ray crystal structure of $SnEt_2$(dapt)[H_2dapt = 2,6-diacetylpyridine bis(2-thenoylhydrazone)], J. Chem. Soc., Dalton Trans (1989) 289–293.

[50] P. Šveca, K. Bartoš, Z. Růžičková, P. Cuřínovác, L. Dušekd, J. Tureke, F. De Profte, A. Růžička, C,N-chelated organotin(IV) azides: synthesis, structure and use within the click chemistry, New J. Chem 40 (2016) 5808–5817.